The Hsp70 interdomain linker is a dynamic switch that enables allosteric communication between two structured domains

Received for publication, March 31, 2017, and in revised form, July 19, 2017 Published, Papers in Press, July 28, 2017, DOI 10.1074/jbc.M117.789313

Charles A. English[‡], Woody Sherman[‡§¶1], Wenli Meng[‡], and Lila M. Gierasch[‡¶2]

From the Departments of [‡]Biochemistry and Molecular Biology and [¶]Chemistry, University of Massachusetts, Amherst, Massachusetts 01003 and [§]Schrödinger Inc., Cambridge, Massachusetts 02142

Edited by Wolfgang Peti

Hsp70 molecular chaperones play key roles in cellular protein homeostasis by binding to exposed hydrophobic regions of incompletely folded or aggregated proteins. This crucial Hsp70 function relies on allosteric communication between two well-structured domains: an N-terminal nucleotide-binding domain (NBD) and a C-terminal substrate-binding domain (SBD), which are tethered by an interdomain linker. ATP or ADP binding to the NBD alters the substrate-binding affinity of the SBD, triggering functionally essential cycles of substrate binding and release. The interdomain linker is a well-structured participant in the interdomain interface in ATP-bound Hsp70s. By contrast, in the ADP-bound state, exemplified by the *Escherichia coli* Hsp70 DnaK, the interdomain linker is flexible. Hsp70 interdomain linker sequences are highly conserved; moreover, mutations in this region compromise interdomain allostery. To better understand the role of this region in Hsp70 allostery, we used molecular dynamics simulations to explore the conformational landscape of the interdomain linker in ADP-bound DnaK and supported our simulations by strategic experimental data. We found that while the interdomain linker samples many conformations, it behaves as three relatively ordered segments connected by hinges. As a consequence, the distances and orientations between the NBD and SBD are limited. Additionally, the C-terminal region of the linker forms previously unreported, transient interactions with the SBD, and the predominant linker-docking site is available in only one allosteric state, that with high affinity for substrate. This preferential binding implicates the interdomain linker as a dynamic allosteric switch. The linker-binding site on the SBD is a potential target for small molecule modulators of the Hsp70 allosteric cycle.

This work was supported by the University of Massachusetts (Amherst, MA) and Schrödinger Inc. through an Academic-Industry Fellowship as well as NIGMS, National Institutes of Health, Grants 5R01GM027616-37 and 1R35GM118161-01 (to L. M. G.). The authors declare that they have no conflicts of interest with the contents of this article. The content is solely the responsibility of the authors and does not necessarily represent the official views of the National Institutes of Health.

This article contains supplemental Table S1 and Figs. S1–S3.

[1] Present address: Silicon Therapeutics, 300 A St., Boston, MA 02210.

[2] To whom correspondence should be addressed: Dept. of Biochemistry and Molecular Biology, University of Massachusetts, Amherst, MA 01003. Tel.: 413-545-6094; Fax: 413-545-1289; E-mail: gierasch@biochem.umass.edu.

Hsp70[3] molecular chaperones maintain cellular protein homeostasis by binding to exposed hydrophobic regions of incompletely folded and aggregated proteins and then allosterically shifting between states with high and low substrate affinities in response to the binding of adenine nucleotides. This mechanism enables Hsp70 chaperones to facilitate initial folding of newly synthesized proteins, protect substrates from aggregation, and facilitate assembly of complexes. Extensive work using the *Escherichia coli* Hsp70 DnaK as a model has shown that when Hsp70 chaperones are bound to ADP, their N-terminal nucleotide-binding domain (NBD) is disengaged ("undocked") from the C-terminal substrate-binding domain (SBD), the helical lid of the SBD is closed over the substrate-binding cleft, and the substrate on/off binding rates to the SBD are slow with high binding affinity for substrates (1–3). By contrast, when the chaperone is bound to ATP, the NBD docks onto the SBD, and interfaces are formed between the β-subdomain of the SBD and the NBD, and between the helical lid and the NBD (Fig. 1*A*) (4, 5).

The NBD and SBD of Hsp70s are connected via an interdomain linker. The interdomain linker participates in the allosteric transitions between the docked and undocked states in several ways. First, in the docked, ATP-bound state, a portion of the linker containing a highly conserved, hydrophobic sequence (VLLL in DnaK) binds to a pocket beneath the crossing helices of the NBD and adopts a β-strand conformation, adding to a small β-sheet in subdomain IIA of the actin-like fold of the NBD (4, 5) (Fig. 1*B*). Substrate binding to the SBD results in an increase in the ATPase activity of the NBD, thus enabling rapid transitions between the high- and low-affinity states. Strikingly, binding of the linker to the NBD is sufficient to shift the NBD conformation and stimulate the rate of hydrolysis of ATP to ADP even in the absence of the SBD (3, 6), showing that the binding of the linker to the NBD is a key event in allosteric communication between the NBD and the SBD. Second, the linker contributes to allosteric functioning in the undocked state by acting as a flexible tether and enabling the domains to behave as independent units. The tethered domains adopt conformational states that are essentially the same as the structures

[3] The abbreviations used are: Hsp70, 70-kDa heat shock protein; NBD, nucleotide-binding domain; SBD, substrate-binding domain; MD, molecular dynamics; MSA, multiple-sequence alignment; DS, dominant state; PDB, Protein Data Bank.

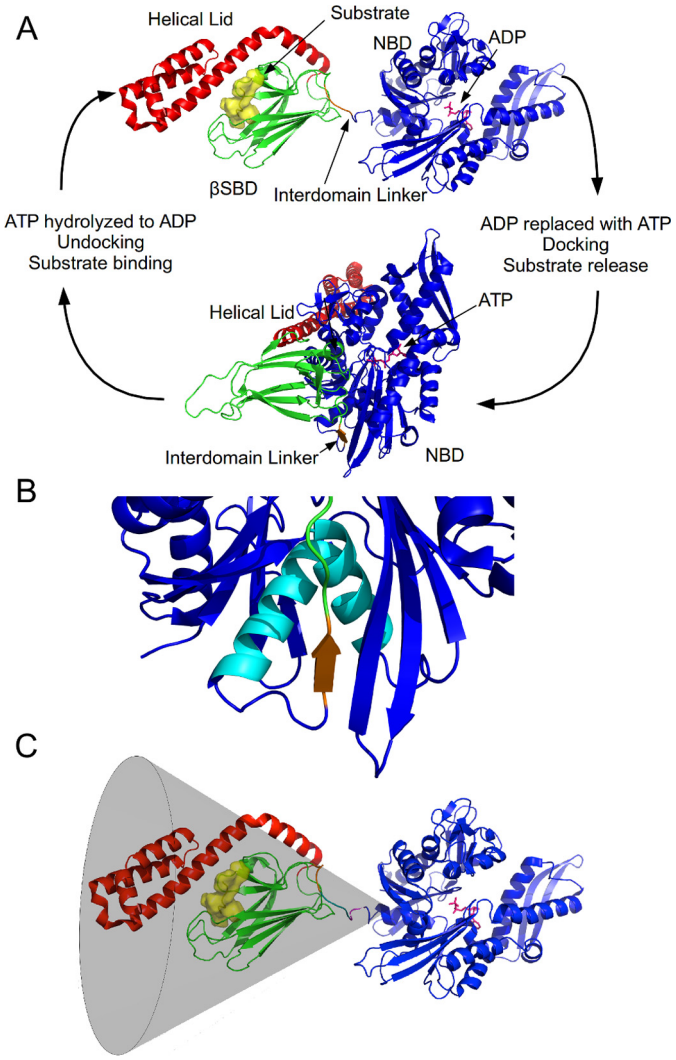

Figure 1. *A*, the allosteric cycle of DnaK showing the undocked/ADP-bound state (*top*) and docked/ATP-bound state (*bottom*) (PDB codes 2KHO (7) and 4JN4 (5), respectively). *B*, *close-up view* of the docked linker in the ATP-bound state, corresponding to the region labeled in the bottom structure in *A*. The crossing helices are *highlighted* in *cyan*. *C*, the relative orientations of the NBD and SBD in ADP-bound DnaK are restricted to the *gray cone*, based on NMR analysis (7). In all images, the NBD is *colored blue*, βSBD is *green*, the VLLL linker sequence is *orange*, and the α-helical lid is *red*. The nucleotides, ATP in the docked state, and ADP in the undocked state, are *colored pink*. The substrate (*superimposed* from PDB entry 1DKZ (17)) is *colored yellow*.

they assume when isolated from the rest of the system (3, 7). When acting as a tether, the interdomain linker samples an ensemble of structures, apparently behaving as an intrinsically disordered segment: It is proteolytically labile (8, 9) and gives rise to sharp resonances with little dispersion in NMR spectra (3, 10). However, the linker imposes some restrictions on the relative orientations of the NBD and SBD, as shown by NMR analysis of the ADP-bound DnaK in which interdomain paramagnetic relaxation data were consistent with restriction of NBD and SBD relative orientations to a 35° cone (7) (Fig. 1*C*). Teleologically, one could argue that these restrictions limit the amount of conformational space searched to find the transition pathway to the docked state (*i.e.* reducing the entropy loss upon interconverting between states, thereby facilitating the transitions). Hence, the conformational sampling of the interdomain linker must be finely tuned throughout the Hsp70 allosteric cycle.

A detailed picture of the conformational landscape of the Hsp70 interdomain linker is lacking, particularly in the ADP-bound state, where the linker populates an ensemble of conformations, and the adjacent domains are structured but undocked. It is crucial that the linker behavior be examined in the presence of its neighboring domains, because transient interactions such as those proposed based on mutagenesis of the linker (6) may play an important role in shaping the linker conformational ensemble. Thus, the full Hsp70 molecule (70 kDa) must be analyzed to derive an accurate structural ensemble of the interdomain linker in the undocked state. To retain the key atomic level details necessary to precisely characterize interfaces between the linker and the domains, we used all-atom molecular dynamics (MD) of the intact DnaK system. Other groups have deployed powerful computational approaches to pose questions about the DnaK system, and their findings have been interpreted in terms of its allosteric function, although the linker conformational landscape was not the primary focus of these studies. For example, Morra and coworkers (11, 12) simulated the initial steps in the allosteric transition of DnaK from its ADP-bound to its ATP-bound state. For ADP and substrate-bound DnaK (12), these authors observed a state with the two domains collapsed on one another and several contacts between the linker and the SBD. Stetz and Verkhiver (13, 14) applied a novel network model that incorporates evolutionary sequence information and MD-derived trajectories to elucidate potential allosteric communication mechanisms. Their approach identified several candidate residue interaction patterns that may be important in allostery. Finally, Penkler *et al.* (15) used MD to study structural perturbations brought about by the binding and unbinding of nucleotides and substrates. They report the residues that undergo the largest, induced structural perturbations and infer that these are probably critical to allostery. Among these were residues Lys^{387}–Val^{389}, Leu^{391}, and Asp^{393} in the linker, consistent with the present work. They also reported several linker interactions with the SBD, but no specific contacts were described. Here, we have focused on the conformational behavior that underlies a crucial role of the linker in allostery in the elusive conformationally dynamic undocked state of DnaK.

Our work reveals that the DnaK interdomain linker conformational landscape comprises a limited set of conformations, even in the undocked, ADP-bound state. In addition to the well-defined structure seen in crystal structures of ATP-bound DnaK, in the undocked state, the linker behaves as a hinged tether, with locally ordered segments connected by hinge residues, thus enabling some relative motion of the two tethered domains but restricting both the interdomain distance and the relative orientations of the domains significantly. We further show that in the ADP-bound state of DnaK, the conserved hydrophobic segment of the linker forms specific but transient contacts with the SBD. The picture that emerges from this analysis presents the interdomain linker as a dynamic switch that performs a key role in interdomain allostery through alternative interactions with either the NBD or the SBD and restricted interdomain relative orientations. This improved understand-

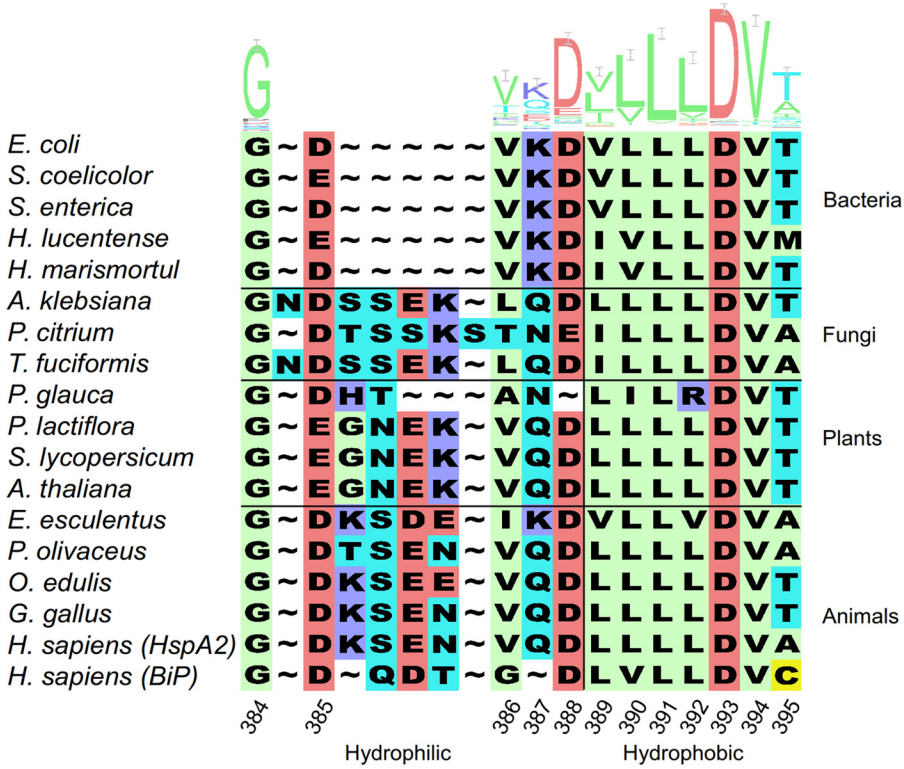

Figure 2. Representative multiple-sequence alignment for interdomain linkers of Hsp70s from a variety of organisms. The *logos* (19) denote how conserved each residue is within the full 640-sequence MSA (18). The division into hydrophilic and hydrophobic regions is denoted at the *bottom*. The residue numbers correspond to those in DnaK.

ing of the interdomain linker interactions broadens the potential to interfere in Hsp70 function by targeting specific sites with small molecule modulators, which could be used as chemical probes or as the basis for the development of novel therapeutics. In addition, our observations offer an explanation for several evolutionarily conserved features of the interdomain linker.

Results

Hsp70 interdomain linkers exhibit high conservation and characteristic sequence regions

Based on inspection of prokaryotic Hsp70 sequences and domain X-ray crystal structures, we defined the DnaK linker region as ^{384}GDVKDVLLLDVT^{395} because Gly^{384} terminates a highly conserved α-helix in the NBD (PDB code 1DKG) (16), and the residue following Thr^{395} (Pro^{396}) is the first residue belonging to secondary structure associated with the SBD (PDB code 1DKX) (17). The electron density of the linker is not well-resolved in X-ray crystal structures of DnaK domains, arguing that it is a flexible interdomain tether. We compared 640 Hsp70 interdomain linker sequences using a multiple-sequence alignment (MSA) (18). We find that many eukaryotic interdomain linkers are longer than those from prokaryotic Hsp70s; the increased length arises from an insertion of three residues between positions 384 and 387 and one residue between residue 387 and 388 (numbered according to the *E. coli* DnaK sequence). A few fungal Hsp70 interdomain linker sequences are one residue longer than most eukaryotic, and a few are outliers (*e.g.* the sequence from white spruce is one residue longer than the sequence of prokaryotes). Fig. 2 shows a representative set of Hsp70 interdomain linker sequences and the sequence conservation logos (19) calculated for the full MSA. Many residues in the linker sequence are highly conserved. In particular, Gly^{384}, Asp^{388}, Leu^{391}, Asp^{393}, and Val^{394} are over 80% conserved in the MSA. Two regions can readily be identified in the interdomain linker: first, an N-terminal region that is predominantly hydrophilic, ^{384}GDVKD^{388} in DnaK. This region is moderately conserved among Hsp70s, with variation in length but retention of hydrophilic character with the exception of Val^{386}, which is highly conserved (68% hydrophobic). This region is followed by a strongly conserved (at least 90% conserved in residue type) hydrophobic region, ^{389}VLLLDVT^{395} in DnaK. In the last three-residue region, ^{393}DVT^{395} in *E. coli* DnaK, the DV sequence is nearly 100% conserved, and Thr^{395} is nearly always Thr or Ala, with occasional substitution by other small uncharged, non-aromatic residues. Secondary structure predictions for the linker sequence suggest that whereas the hydrophilic region is random coil, the ^{389}VLLLD^{393} region is predicted to be an extended strand (20).

The interdomain linker in the ATP-bound Hsp70 state adopts a well-defined structure and is an integral component of the interdomain interface

In the ATP-bound structures of DnaK (PDB codes 4B9Q (4) and 4JN4 (5)) and the human Hsp70 that resides in the endoplasmic reticulum (BiP) (PDB code 5E84 (21)), the interdomain linker adopts a well-defined structure in which the conserved C-terminal hydrophobic sequence, VLLL (Fig. 2), is incorporated into subdomain IIA of the NBD as an antiparallel fourth β-strand on the edge of the small sheet (Fig. 1*B*). The crystal

structure of the ATP-bound form of BiP also provides a picture of the conformation adopted by a mammalian interdomain linker with its additional five residues in the hydrophilic-dominated region (21). The hydrophilic-dominated region of the linker for both Hsp70s forms a solvent-exposed loop (Fig. 1*B*) with a fold that has been termed a "niche-4l motif" (22). This motif generally allows for metal ion binding, but in this case, it enables a large amount of the surface area of the loop to be solvent-exposed. In contrast, the hydrophobic-dominated region adopts a β-sheet configuration. This arrangement shields the hydrophobic region from the solvent.

It is noteworthy that all of these structures represent a low-energy state adopted when the given Hsp70 is ATP-bound and under the conditions of crystallization (*i.e.* in the crystal lattice and for the particular construct crystallized). In one structure (PDB code 4JN4 (5)), several mutations were incorporated into loops of DnaK to facilitate crystallization of the ATP-bound form (5), and in the other structure (PDB code 4B9Q (4)), a disulfide was introduced between the α-helical lid and the NBD to achieve crystallization. To verify that the linker would adopt the conformation seen in these crystal structures when in the context of wild-type DnaK and relieved of the constraints of the crystal lattice, we ran 15-ns MD simulations to relax the docked ATP-bound crystal structure of full-length, wild-type DnaK with implicit solvent (see "Experimental procedures" for details). We found that the linker retains the backbone conformation seen in the crystal structures, and most side chains do not change their conformations significantly, with the exception of the Lys^{387} side chain, which fluctuated among several solvent-exposed conformations.

The interdomain linker in ADP-bound DnaK samples a restricted set of conformations and interacts with a pocket on the substrate-binding domain

To explore the conformational ensemble of the interdomain linker in the context of the NBD and SBD, we ran all-atom MD simulations on the undocked ADP-bound state of DnaK (for details, see "Experimental procedures"). A major consideration in calculating the conformational landscapes for molecules as large as DnaK is the completeness of the conformational exploration. To assess whether our simulations fully explored conformational space without becoming trapped in a local minimum, we ran three independent trajectories from different starting structures. The first trajectory, lasting 600 ns, started from the reported NMR-derived ADP-bound DnaK structure (PDB code 2KHO) (7). In the second, a 200-ns simulation, the initial NBD and SBD structures were unchanged, but the linker was computationally altered to an α-helical conformation. A third, short (200-ns) simulation was run with the linker initially in a β-sheet conformation, again retaining the NBD and SBD structures from PDB entry 2KHO (7) while altering their relative orientations. In all three trajectories, the linker rapidly (within 25 ns of the start of the simulation) began to populate the same states (supplemental Fig. S1). Furthermore, no new states were populated in any of the additional simulations, suggesting that the relevant regions of the conformational landscape were fully explored.

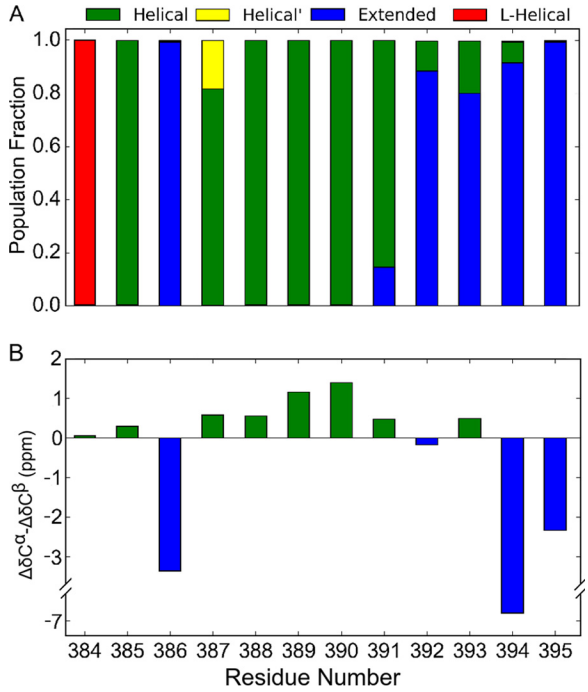

Figure 3. Predominant secondary structures adopted by each linker residue when the linker is part of ADP-bound DnaK. *A*, the population is given as a fraction of the configurations sampled by MD. Extended structure is defined by φ dihedral angles between $-200°$ (160°) and 25° and ψ dihedral angles between 50 and $-140°$ (220°). Helical structure is characterized by φ dihedral angles between -110 and 25° and ψ angles between -125 and 85°. Lys^{387} populates two substates. One (*Helical*) has canonical φ, ψ values, and the other (*Helical'*) is distorted with a φ angle between -180 and $-110°$. Left-handed helix conformations are defined by φ dihedral angles between 25 and 160° and ψ dihedral angles between -60 and 100°. Dihedral angles not within the ranges described above are considered "other". These other states are included in the total population count. *B*, $\Delta\delta C\alpha - \Delta\delta C\beta$ secondary chemical shifts (23) from residue 384 to 395 in the two-domain construct, DnaK(1–552), in the ADP-bound state. Positive values indicate α-helical propensity, and negative values indicate β-structure propensity. Values greater than 2 ppm or less than -2 ppm suggest fully formed secondary structure, whereas smaller deviations often indicate partial secondary structure propensities.

The overall ADP–DnaK structure behaved very similarly in our MD trajectories as it did in the model that emerged from NMR studies carried out by Bertelsen *et al.* (7) (supplemental Table S1). In particular, the NBD and SBD were observed to reorient with respect to each another as though tethered by a flexible linker; however, in agreement with the conclusions of the NMR studies, our careful analysis of the conformational explorations of the linker revealed that the relative motion of the two domains was restricted. Moreover, the linker end-to-end distance varied from 15 to 30 Å with 95% of the population between 15 and 19 Å in a near Gaussian distribution (see supplemental Fig. S2). Thus, the conformational states populated by the interdomain linker play a dual function: They restrict both the relative orientations sampled by the NBD and SBD and the interdomain distance fluctuations. The predominant secondary structures adopted by linker residues are shown in Fig. 3. For comparison purposes, we also simulated the linker in the absence of the NBD and SBD. We found that the interdomain linker in the absence of any influence from neighboring domains has a high propensity to adopt a significant amount of helical secondary structure (supplemental Fig. S3), indicating that it possesses its own inherent structural properties and that

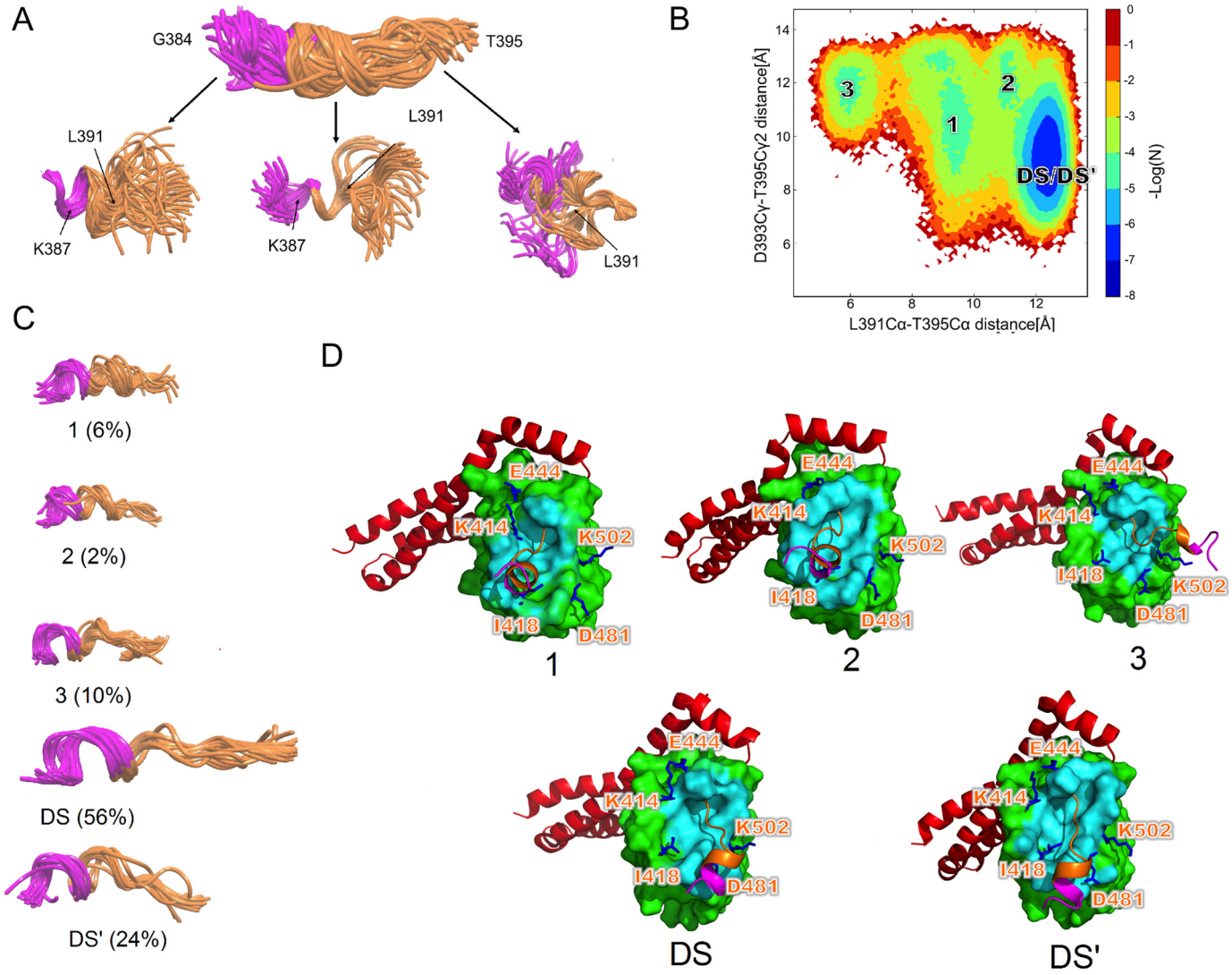

Figure 4. *A*, overlay of linker conformations based on minimizing root mean square deviation using all backbone atoms (*top*) and then (from *left* to *right*) by all backbone atoms for the hydrophilic, central hydrophobic, and C-terminal regions, separately (*bottom*). *B*, conformational landscape projected over two intralinker atom distance pairs. The conformational landscape is a 2D histogram with each bin normalized by taking the negative logarithm of the total bin population. Each basin is *labeled* by the state it corresponds to. *C*, overlays by all backbone atoms for each basin in the conformational landscape. Each overlay is *labeled* by the basin it occupies. *D*, linker–SBD conformation for each of the minima, with the SBD area contacting the linker indicated (within 5 Å, highlighted in *cyan*). Key residues are highlighted in *blue*, SBD is *green*, the hydrophobic linker region is *orange*, and the hydrophilic region is *magenta*.

its behavior in the full chaperone is strongly influenced by adjacent NBD and SBD.

Although it is somewhat structurally restricted, the interdomain linker in ADP-bound DnaK resembles an intrinsically disordered region in that many conformational states are visited over the course of the trajectory. The conformational ensemble of the linker is depicted in an overlay of 60 structures from every 10 ns of the 600-ns MD trajectory (Fig. 4*A*, *top*). Strikingly, when different regions of the linker were superimposed separately, we found that the apparently disordered linker is in fact a composite of three relatively ordered regions with persistent conformational preferences (see Fig. 4*A*): residues 384–386 (part of the N-terminal hydrophilic region); residues 388–390 (the hydrophobic central region); and residues 392–395 (encompassing the conserved C-terminal sequence LDVT). Between the ordered regions are hinge points (at residues Lys^{387} and Leu^{391}), which allow the linker to adopt multiple conformations that comprise an ensemble, but a restricted ensemble. We overlaid linker conformations to determine how many distinct states are allowed under the restrictions imposed by the hinge residues. From the overlays in Fig. 4*A*, we see that the hydrophobic central region is the most ordered of the three regions and adopts an α-helical conformation. The N-terminal region possesses some limited flexibility, mostly concentrated in the initial two residues, Gly^{384} and Asp^{385}, and samples (φ, ψ) angles near (80°, 20°) and (−75°, −25°), respectively. By contrast, the C-terminal region clearly comprises alternative conformational states, although its overlay shows some clustering. By projecting the sampled conformational space on coordinates that sensitively report on excursions of this region, we found one major energy minimum and three minor minima (Fig. 4*B*). The dominant state (DS) represents 80% of the population and may therefore be the most relevant state for allosteric communication. The overlays for each of the linker energy

minima are shown in Fig. 4*C* along with their populations. Note that the dominant state can be subdivided into a state comprising 56% of the population (denoted DS), in which the C-terminal residues 392–395 are in an extended conformation, and a minor substate (denoted DS′ and comprising 24% of the population), in which residue 392 is helical. Importantly, the tendency of the linker residues to populate well-defined conformational regions of φ, ψ space despite an overall relatively disordered character for the full segment, which we found in our simulations, is experimentally supported by NMR properties of these residues. It was possible to assign diagnostic resonances corresponding to most of the linker residues in a two-domain construct of ADP-bound DnaK. Correlations of $\Delta\delta C\alpha - \Delta\delta C\beta$ with secondary structure (23) thus provided experimental support for the biased sampling of conformational space seen in our MD simulations. As shown in Fig. 3*B*, the bias in φ, ψ angles populated as indicated by NMR data correlates remarkably well with the results of simulations. Consecutive positive $\Delta\delta C\alpha - \Delta\delta C\beta$ values ranging from 0.5 to 1.4 ppm are observed for residues Lys^{387}–Leu^{391}, indicating α-helical propensities in this region. By contrast, residues Val^{386}, Val^{394}, and Thr^{395} exhibit significantly negative $\Delta\delta C\alpha - \Delta\delta C\beta$ values, suggesting that these residues adopt β-structure φ, ψ angles, consistent with our simulation results.

Significantly, the interdomain linker in ADP-bound DnaK, which was thought to behave quite independently, actively participates in interactions with each of the two attached domains. There are non-persistent contacts between the hydrophilic region of the linker and the NBD that periodically form and break on the nanosecond time scale. Nearly all of these contacts are formed with residues in the NBD loop, beginning at Met^{19} and ending at Thr^{23}. More notable are a set of previously uncharacterized contacts with the SBD that are more persistent than those formed with the NBD. Because these interactions involve principally the C-terminal domain interface region of the linker (residues 392–395), we have analyzed them in terms of the substates adopted by this region of the linker as described above and shown in Fig. 4 (*B* and *C*). When in the DS state (including DS′), this region of the linker interacts with a pocket situated on the NBD-facing side of the SBD (Fig. 5*A*). Strikingly, in one of the crystal forms of the SBD, there is a packing interaction in which this pocket is occupied by the linker of an adjacent molecule (PDB code 1DKX (17) (Fig. 5*B*). Importantly, this pocket is present when the SBD is in its high substrate affinity (ADP-bound) conformation but absent when the SBD is in the low substrate affinity (ATP-bound) conformation (Fig. 5, *C* and *D*), arguing for a role for the interaction with this pocket in the allosteric energy landscape. Indeed, a small molecule inhibitor of DnaK and Hsp70, PET-16, was found to bind to this pocket (24) (Fig. 5*E*). Additionally, an early NMR study of an SBD construct reported that a model substrate peptide termed NR may also bind to this pocket (25) (Fig. 5*F*). We also examined how the minor linker populations that occupy energy minima 1, 2, and 3 interact with the SBD and noted differences in how these minima interact with the SBD *versus* the dominant state (Fig. 4*D*). Energy minima 1 and 2 corresponded to conformations in which the linker was placed in closer proximity to the NBD binding groove, suggesting that these states may be important

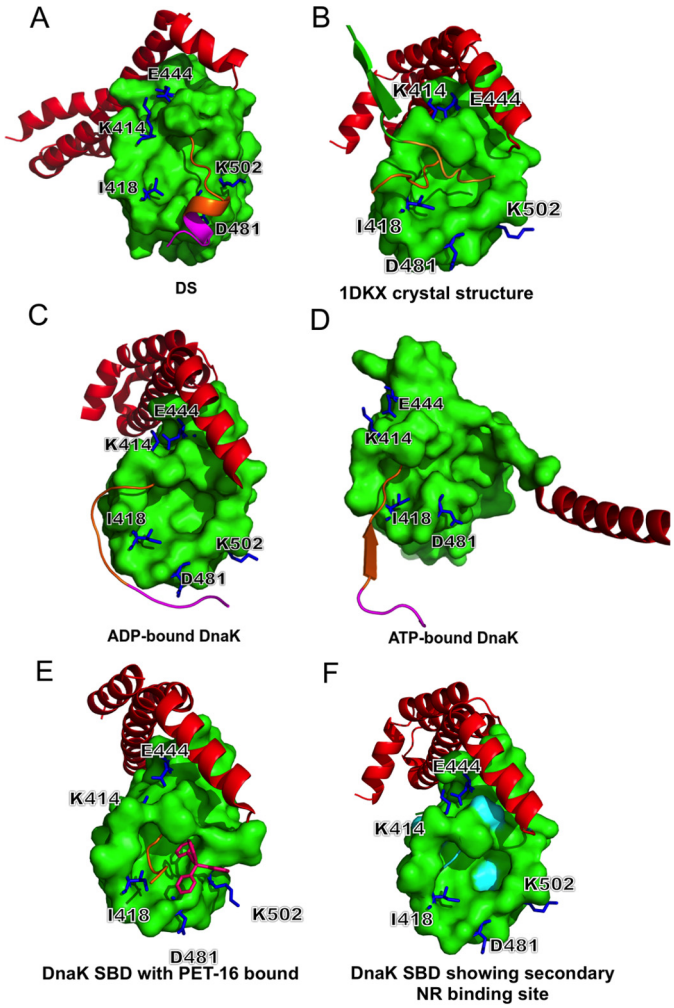

Figure 5. *A*, linker interaction with the SBD pocket in the predominant state from MD simulations. Depictions of the allosteric opening and closing of this pocket follow. *B*, the open pocket in the SBD crystal structure (PDB code 1DKX (16)) partially occupied by the neighboring molecule's linker; *C*, the open arrangement as found in ADP-bound DnaK (PDB code 2KHO (7)); *D*, the closed arrangement as found in ATP-bound DnaK (PDB code 4JN4 (5)); *E*, structure of DnaK SBD with PET-16 (*fuchsia*) bound to the SBD pocket (PDB code 4R5G) (24); *F*, SBD pocket with residues highlighted in *cyan*, which, from an early NMR study (25), constitute a secondary binding site for model substrate peptides. Key charged residues are *highlighted* in *blue* and *labeled*. The *color scheme* is the same as in Figs. 1 and 4.

during an allosteric transition. Furthermore, for the allosteric transition to occur, the SBD pocket must close to reach the ATP-bound configuration. Because minima 1 and 2 (as well as 3) remove the linker from part of the pocket, these linker arrangements would more rapidly facilitate the closing of the pocket.

Discussion

The allosteric cycle of Hsp70s underlies their many biological and physiological functions. Through the nucleotide-mediated cycle of conformational changes, Hsp70s interact with their substrates and co-chaperones so as to bind and release substrates in an ATP-dependent manner. Structural data for the component domains of the *E. coli* Hsp70 DnaK and for the ATP-bound state of DnaK and the mammalian endoplasmic reticulum Hsp70 (BiP) have shown that a major conformational

change occurs during the allosteric cycle. Work from many laboratories has shown that Hsp70s are modular nanomachines and that the ability of each of their domains to sample alternative conformations enables the allosteric switch seen in DnaK between ATP-bound (docked) and ADP-bound (undocked) states. However, it has remained a mystery how interdomain communication is achieved in Hsp70s.

In crystal structures of ATP-bound DnaK, the interdomain linker is a well-folded participant in the large interdomain interface, with the VLLL that resides near the C terminus of the interdomain linker adopting a β-strand conformation and joining a sheet in NBD subdomain IIA. The ATP-mediated conformational change of the NBD opens a pocket under the crossing helices and shifts the β-sheet in subdomain IIA, allowing the linker to fold into the interdomain interface. Docking of the VLLL brings the NBD and SBD closer to one another. The ability of the SBD to sample two conformations, one of which can productively interact with the interface presented by the ATP-bound NBD and the interdomain linker, is at the core of the allosteric response of DnaK to ATP binding.

But what is the role of the interdomain linker in the ADP-bound state? The identity of the NMR spectral signatures of isolated NBD and SBD to the spectral signatures of these domains in ADP-bound DnaK (3, 7) along with the proteolytic lability of the interdomain linker in DnaK (8, 9) have painted a picture of two structured domains linked by a conformationally unrestricted tether in ADP-bound DnaK. An in-depth NMR study using a combination of residual dipolar couplings and paramagnetic relaxation enhancements concluded that the relative motion of the NBD and SBD in ADP-bound DnaK was in fact restricted to a 35° cone (7). The current study suggests that the favored linker conformations may contribute to the observed restrictions of the relative positions of the two domains. This observation together with several results showing the intolerance of the interdomain linker to mutation (26) raise the possibility that the linker is performing a more complex role in allostery than previously thought. The present study has now provided a clearer picture of the interdomain linker's behavior in the ADP-bound state of DnaK and allowed us to compare this with the ATP-bound docked state and obtain a deeper understanding of the role of the Hsp70 linker in interdomain allosteric communication. The ability of the linker to interconvert between a well-folded state in ATP-bound DnaK and a flexible tether plays a significant role in interdomain communication. The present approach based on MD simulations of the conformationally dynamic interdomain linker in ADP-bound DnaK has provided new insight into this elusive state.

Our examination of conservation in the interdomain linker pointed to two regions of differing hydrophobicity: the first five amino acids, which are mainly hydrophilic, and the next seven residues, which are predominantly hydrophobic. In our MD simulations of ADP-bound DnaK and analysis of the ATP-bound DnaK structure, we can see that the solvent-accessible surface presented by each of these two regions is consistent with their relative hydrophobicity in both allosteric states. Most striking and unanticipated were the results from our simulations of ADP-bound DnaK showing that the interdomain linker is not as flexible as previously thought, but instead is made up of three locally ordered segments connected by hinges. Our analysis has thus enabled us to understand the key role of the interdomain linker in restricted orientational sampling of the two domains. Simulations of the linker alone revealed a preference for relatively ordered conformations that is intrinsic to its sequence. Importantly, the intrinsic conformational preferences of the linker are modulated by the SBD and NBD. In addition, the fact that the interdomain linker interacts persistently with the SBD via sites that would only be available in the high substrate affinity state of the SBD offers exciting new insights into the allosteric mechanism of DnaK.

Critically, the domain interface region that we identify from residue 392 to 395 and the residues this region contacts on the SBD surface could be prime targets for small molecule binding with the intent of modulating the allosteric cycle as the linker shields critical residues in the NBD–SBD docked state interface from the solvent and the NBD. MD trajectories show repeated formation and breaking of contacts between specific linker and SBD residues. This suggests that the linker–SBD interface region and pocket behave like a "fuzzy" complex (27), where interfaces shift due to transient contacts between domains. Although 80% of the population is in a dominant state, the existence of several minor states may play a role in linker function. It is possible that the pocket has evolved to accommodate the linker in multiple arrangements, as opposed to a single "lock and key" fit, although clearly one configuration is highly favored. It is interesting to speculate that because the pocket is no longer accessible upon transition to the ATP-bound state, the existence of multiple transient binding states may contribute to allosteric efficiency, because a strongly bound linker would prevent the pocket's closure.

The question may be asked: To what extent do the MD simulations accurately reflect the conformations sampled by the linker in solution? It is difficult to characterize the linker conformational ensemble experimentally, but we were able to extract the conformationally diagnostic NMR carbon-α and -β chemical shifts of the linker residues from spectra of ADP-bound DnaK and to compare the secondary structure biases that they suggest with the MD simulations to gain insights unobtainable by other means. The results of simulations together with the NMR parameters are not readily used as quantitative measures of populations of conformational states. Rather, we draw from the behaviors seen in the simulations and supported by the NMR data conclusions about conformational behaviors and interactions that are possible for the flexible interdomain linker, and then we use these observations to help explain experimental observations and to push our models in ways that we could not have anticipated without knowledge of the possible conformational sampling. We underline the particular value of this approach when dealing with functionally important yet flexible components of a molecular machine, where we lack direct experimental constraints.

In this way, several new insights about the DnaK interdomain linker were obtained here. The MD-derived conformational landscape of the interdomain linker in the context of ADP-bound DnaK offers an explanation for evolutionary constraints seen in the multiple-sequence alignment of Hsp70 interdomain

linkers and with previous studies in which the linker residues were subjected to mutagenesis (6). The interdomain linker has sequence characteristics that enable it to serve as an allosteric switch. In the well-ordered ATP-bound, docked state of DnaK, it can adopt a specific structure with the N-terminal predominantly hydrophilic region solvent-exposed while the predominantly hydrophobic C-terminal region forms a β-strand. In the β-strand, Leu^{390} and Leu^{392} face the NBD and participate in hydrophobic packing. These two residues need not be hydrophobic, as in the case of the Hsp70 homologue Hsp110, where they are replaced by Ile and Pro, respectively. However, Hsp110's function does not require its interdomain linker to undergo interconversion between alternative conformations (28). Thus, the Hsp110 interdomain linker sequences do not face this additional evolutionary pressure as in the case of the Hsp70. Thus, the preference for leucines at these positions in DnaK may be accounted for by the role of these residues in the ADP-bound state. Finally, the highly conserved Asp^{393} contacts NBD residue Arg^{167}, offering an explanation for the known role of this residue in proper allosteric functioning (6). Alternatively, our results show that the linker can display local order and conformational freedom at hinge sites in the ADP-bound state. The predominantly hydrophilic N-terminal region remains highly solvent-exposed, whereas the predominantly hydrophobic region displays "dual use" of its sequence, in particular due to the high number of leucines. Leucines have a strong propensity to form either α-helical or β-sheet structure (29–31). This conformational malleability may account for the conservation of the VLLL sequence. The adoption of a nascent helix in the N-terminal and central regions of the linker in the ADP-bound state confers rigidity and compacts the linker. This order is exploited to impose restrictions on the relative orientation of the SBD and NBD. Last, the interactions of the interdomain linker, either with the pocket under the crossing helices of the ATP-bound NBD or with pockets present on the high affinity conformation of the SBD in ADP-bound DnaK, involve an overlapping set of residues: Asp^{393}–Thr^{395}. Thus, these residues are under evolutionary pressure to participate in two interfaces, each with its respective set of contacts.

It is of interest to compare our findings with previous simulations of the DnaK allosteric landscape. In their work, Chiappori *et al.* (11, 12) focused on hydrogen-bonding contacts between DnaK structural units to test their hypothesis that hydrogen-bonding networks are key to allostery; the only contact they reported between the linker and the adjacent domains in ADP-bound DnaK was between Thr^{395} in the C-terminal region of the linker and the SBD residue Thr^{416}. This interaction was not observed in our all-atom MD simulations. More direct comparison between contacts in the earlier (11) and more recent (12) studies from this group is not possible because only the hydrogen-bonding interactions are reported. We note, however, that both the ADP-bound and substrate-, ADP-bound forms of DnaK simulated by Chiappori *et al.* (11, 12) were significantly more collapsed than would be consistent with experiments. Stetz and Verkhivker (13, 14) propose that several linker residues are important in allostery based on a combination of evolutionary co-variance and dynamic character. Among these are Gly^{384}, Asp^{385}, Val^{386}, Lys^{387}, Leu^{390}, Asp^{393}, and Thr^{395}, which they propose to be hinge residues, in either forward or reverse allosteric pathways. Our work also points to the importance of these residues, but we find the dynamics of the linker to be better characterized as ordered segments with connecting hinges at Lys^{387} and Leu^{391}. Stetz and Verkhivker (13, 14) also posit that several linker residues interact with the SBD, which is consistent with the observations made here. Similarly, Penkler *et al.* (15) observed linker interactions with the SBD consistent with our observations. At various points in the allosteric cycle, linker residues Lys^{387}–Val^{389} and Leu^{391}–Asp^{393} are able to undergo significant structural perturbations. Although this is similar to our results, we did not find residues Asp^{388} and Val^{389} to be part of a hinge, instead finding that these residues comprise a more ordered region.

Although the roles of several linker residues are becoming clearer based on conformational considerations, it is less clear why Asp^{388} and Asp^{393} are highly conserved. The first expectation upon observing conservation of two negatively charged residues is that they participate in essential electrostatic interactions at some point during the Hsp70 allosteric cycle. These interactions could be within the linker or with either the NBD or SBD. Alternatively, these residues may participate in essential interactions with co-chaperones, such as J-proteins. Indeed, Asp^{393} formed salt-bridge contacts with NBD residue Arg^{167} in the ATP-bound state simulation. However, careful inspection did not point out any electrostatic interactions within DnaK that would explain the conservation of Asp^{388}, suggesting that these residues may interact with co-chaperones or other chaperones. As another possibility, we note that in the linker, Asp^{388} serves as the N-terminal cap of the nascent helix, which might account for its conservation (32). Aspartic acid residues are also common C-terminal caps for β-sheets (33), and Asp^{393} may play this role in the docked state.

Several contacts between the linker and the SBD constitute possible binding sites for small molecules that may selectively target specific Hsp70s. Mutagenesis work has shown that even relatively benign mutations at the NBD–SBD interface can shift the allosteric equilibrium to favor either docked or undocked states (10). The alternative interdomain linker binding pockets on the NBD in the ATP-bound state and on the SBD in the ADP-bound state invite development of allosteric modulators that could bind either pocket. Several reported Hsp70 small molecule modulators may in fact be exploiting these sites (34, 35), but more definitive structural data on their interaction sites are needed to pin this down.

The importance of the interdomain linker for allosteric signal transmission in Hsp70s is undeniable (3, 6), and our enhanced understanding of its role fills one more gap in comprehending how these molecular machines perform their myriad physiological functions. This work should therefore be of great interest to those seeking to use Hsp70s as therapeutic targets for cancer (36–38), Alzheimer's disease (39, 40), and Parkinson's disease (41–43) and the development of novel classes of antibiotics (44). In addition, we also highlight that seemingly flexible linkers are widespread in signaling molecules in biology, and our work illustrates the importance of in-depth study of the roles of these ostensibly flexible units. Delineating their conformational landscapes will shed light on how they

may relay information from one region of a molecule to another.

Experimental procedures

Three MD simulations were set up to explore the conformational landscape of the linker in the undocked state. The first, lasting 600 ns, used the 2KHO PDB entry structure in the undocked form as the initial configuration. The second and third simulation were run to determine whether the simulation from the 2KHO linker starting conformation adequately sampled conformational space and thus was not constrained in a local minimum. We put the linker in conformations that were low-energy regions of φ, ψ space but distant from the linker starting conformation in 2KHO (all α and all β) and ran short simulations. In all cases, the three simulations rapidly adopted the same states, within 1 ns of the start of the simulation. A comparison of dihedral angles for each of the simulations verifies that the same states are sampled. Furthermore, no new states were discovered in any of the additional simulations, suggesting that the conformational landscape is fully explored.

For all MD simulations, we used the Charmm22* force field (45) and the Onufriev-Bashford-Case implicit solvent model (46). We used the OpenMM (47, 48) software package for all MD simulations. We ran the simulations at pH 7 with protonation states determined using PROPKA calculations (49–51). The implicit solvent simulations were run at 300 K using Langevin dynamics with a cutoff distance of 16 Å for all forces, a time coupling constant of 1 ps^{-1}, and an integration time step of 2 fs. We used the Python package MDTraj (52) to analyze the MD trajectories.

NMR spectra of the ADP-bound state of DnaK were obtained on a $^{2}H,^{13}C,^{15}N$-labeled, well-characterized truncated construct, DnaK(1–552), harboring two mutations, L542Y and L543E, in the helical lid to abrogate self-binding and a point mutation, T199A, in the nucleotide-binding site to block hydrolysis (53). The sample was prepared as described previously (10), and TROSY-based HNCA and HNCACB spectra were obtained on a Bruker 600 MHz Avance instrument with a cryoprobe at 26 °C. Assignments were done using standard sequential assignment methods and transferring previous assignments of the DnaK(387–552) construct. The random coil values of Wishart and co-workers (54) were used to calculate secondary chemical shifts.

Author contributions—C. A. E., W. S., W. M., and L. M. G. designed the experiments. C. A. E. performed the simulations and analyzed the corresponding results. W. M. performed the NMR experiments and analyzed the results. C. A. E. wrote the paper with L. M. G. and W. S.

Acknowledgments—We thank Jianhan Chen for advice and suggestions on this work, Eugenia Clerico for critical reading of the manuscript, and Anastasia Zhuravleva for providing NMR data and assignments.

References

1. Mayer, M. P., and Kityk, R. (2015) Insights into the molecular mechanism of allostery in Hsp70s. *Front. Mol. Biosci.* **2,** 58
2. Gierasch, L. M. (2016) Hsp70 molecular machines: versatile modular nanomachines that mediate multiple biological functions. In *Structure and Action of Molecular Chaperones* (Gierasch, L. M., Horwich, A. L., Slingsby, C., Wickner, S., and Agard, D., eds) pp. 1–48, World Scientific, Singapore
3. Swain, J. F., Dinler, G., Sivendran, R., Montgomery, D. L., Stotz, M., and Gierasch, L. M. (2007) Hsp70 chaperone ligands control domain association via an allosteric mechanism mediated by the interdomain linker. *Mol. Cell* **26,** 27–39
4. Kityk, R., Kopp, J., Sinning, I., and Mayer, M. P. (2012) Structure and dynamics of the ATP-bound open conformation of Hsp70 chaperones. *Mol. Cell* **48,** 863–874
5. Qi, R., Sarbeng, E. B., Liu, Q., Le, K. Q., Xu, X., Xu, H., Yang, J., Wong, J. L., Vorvis, C., Hendrickson, W. A., Zhou, L., and Liu, Q. (2013) Allosteric opening of the polypeptide-binding site when an Hsp70 binds ATP. *Nat. Struct. Mol. Biol.* **20,** 900–907
6. Vogel, M., Mayer, M. P., and Bukau, B. (2006) Allosteric regulation of Hsp70 chaperones involves a conserved interdomain linker. *J. Biol. Chem.* **281,** 38705–38711
7. Bertelsen, E. B., Chang, L., Gestwicki, J. E., and Zuiderweg, E. R. (2009) Solution conformation of wild-type *E. coli* Hsp70 (DnaK) chaperone complexed with ADP and substrate. *Proc. Natl. Acad. Sci. U.S.A.* **106,** 8471–8476
8. Buchberger, A., Theyssen, H., Schröder, H., McCarty, J. S., Virgallita, G., Milkereit, P., Reinstein, J., and Bukau, B. (1995) Nucleotide-induced conformational changes in the ATPase and substrate binding domains of the DnaK chaperone provide evidence for interdomain communication. *J. Biol. Chem.* **270,** 16903–16910
9. Kamath-Loeb, A. S., Lu, C. Z., Suh, W. C., Lonetto, M. A., and Gross, C. A. (1995) Analysis of three DnaK mutant proteins suggests that progression through the ATPase cycle requires conformational changes. *J. Biol. Chem.* **270,** 30051–30059
10. Zhuravleva, A., Clerico, E. M., and Gierasch, L. M. (2012) An interdomain energetic tug-of-war creates the allosterically active state in Hsp70 molecular chaperones. *Cell* **151,** 1296–1307
11. Chiappori, F., Merelli, I., Colombo, G., Milanesi, L., and Morra, G. (2012) Molecular mechanism of allosteric communication in Hsp70 revealed by molecular dynamics simulations. *PLoS Comput. Biol.* **8,** e1002844
12. Chiappori, F., Merelli, I., Milanesi, L., Colombo, G., and Morra, G. (2016) An atomistic view of Hsp70 allosteric crosstalk: from the nucleotide to the substrate binding domain and back. *Sci. Rep.* **6,** 23474
13. Stetz, G., and Verkhivker, G. M. (2015) Dancing through life: molecular dynamics simulations and network-centric modeling of allosteric mechanisms in Hsp70 and Hsp110 chaperone proteins. *PLoS One* **10,** e0143752
14. Stetz, G., and Verkhivker, G. M. (2017) Computational analysis of residue interaction network and coevolutionary relationships in the Hsp70 chaperones: a community-hopping model of allosteric regulation communication. *PLoS Comput. Biol.* **13,** e1005299
15. Penkler, D., Sensoy, Ö., Atilgan, C., and Tastan Bishop, Ö. (2017) Perturbation-response scanning reveals key residues for allosteric control in Hsp70. *J. Chem. Inf. Model.* **57,** 1359–1374
16. Harrison, C. J., Hayer-Hartl, M., Di Liberto, M., Hartl, F., and Kuriyan, J. (1997) Crystal structure of the nucleotide exchange factor GrpE bound to the ATPase domain of the molecular chaperone, DnaK. *Science* **276,** 431–435
17. Zhu, X., Zhao, X., Burkholder, W. F., Gragerov, A., Ogata, C. M., Gottesman, M. E., and Hendrickson, W. A. (1996) Structural analysis of substrate binding by the molecular chaperone DnaK. *Science* **272,** 1606–1614
18. Smock, R. G., Rivoire, O., Russ, W. P., Swain, J. F., Leibler, S., Ranganathan, R., and Gierasch, L. M. (2010) An interdomain sector mediating allostery in Hsp70 molecular chaperones. *Mol. Syst. Biol.* **6,** 414
19. Crooks, G. E., Hon, G., Chandonia, J.-M., and Brenner, S. E. (2004) WebLogo: a sequence logo generator. *Genome Res.* **14,** 1188–1190
20. Rost, B., and Sander, C. (1994) Combining evolutionary information and neural networks to predict protein secondary structure. *Proteins* **19,** 55–72

21. Yang, J., Nune, M., Zong, Y., Zhou, L., and Liu, Q. (2015) Close and allosteric opening of the polypeptide-binding site in a human Hsp70 chaperone BiP. *Structure* **23,** 2191–2203
22. Torrance, G. M., Leader, D. P., Gilbert, D. R., and Milner-White, E. J. (2009) A novel main chain motif in proteins bridged by cationic groups: the niche. *J. Mol. Biol.* **385,** 1076–1086
23. Marsh, J. A., Singh, V. K., Jia, Z., and Forman-Kay, J. D. (2006) Sensitivity of secondary structure propensities to sequence differences between α- and γ-synuclein: implications for fibrillation. *Protein Sci.* **15,** 2795–2804
24. Leu, J. I. J., Zhang, P., Murphy, M. E., Marmorstein, R., and George, D. L. (2014) Structural basis for the inhibition of HSP70 and DnaK chaperones by small-molecule targeting of a C-terminal allosteric pocket. *ACS Chem. Biol.* **9,** 2508–2516
25. Wang, H., Kurochkin, A. V., Pang, Y., Hu, W., Flynn, G. C., and Zuiderweg, E. R. (1998) NMR solution structure of the 21 kDa chaperone protein DnaK substrate binding domain: a preview of chaperone-protein interaction. *Biochemistry* **37,** 7929–7940
26. Han, W., and Christen, P. (2001) Mutations in the interdomain linker region of DnaK abolish the chaperone action of the DnaK/DnaJ/GrpE system. *FEBS Lett.* **497,** 55–58
27. Tompa, P., and Fuxreiter, M. (2008) Fuzzy complexes: polymorphism and structural disorder in protein–protein interactions. *Trends Biochem.* **33,** 2–8
28. Liu, Q., and Hendrickson, W. (2007) Insights into Hsp70 chaperone activity from a crystal structure of the yeast Hsp110 Sse1. *Cell* **131,** 106–120
29. Chou, P. Y., and Fasman, G. D. (1978) Empirical predictions of protein conformation. *Annu. Rev. Biochem.* **47,** 251–276
30. Swindells, M. B., MacArthur, M. W., and Thornton, J. M. (1995) Intrinsic φ, ψ propensities of amino acids, derived from the coil regions of known structures. *Nat. Struct. Mol. Biol.* **2,** 596–603
31. Kathuria, S. V., Chan, Y. H., Nobrega, R. P., Özen, A., Matthews, C. R. (2016) Clusters of isoleucine, leucine, and valine side chains define cores of stability in high-energy states of globular proteins: sequence determinants of structure and stability. *Protein Sci.* **25,** 662–675
32. Aurora, R., and Rose, G. D. (1998) Helix capping. *Protein Sci.* **7,** 21–38
33. Farzadfard, F., Gharaei, N., Pezeshk, H., and Marashi, S. A. (2008) β-Sheet capping: signals that initiate and terminate β-sheet formation. *J. Struct. Biol.* **161,** 101–110
34. Goloudina, A. R., Demidov, O. N., and Garrido, C. (2012) Inhibition of HSP70: a challenging anti-cancer strategy. *Cancer Lett.* **325,** 117–124
35. McLean, P. J., Klucken, J., Shin, Y., and Hyman, B. T. (2004) Geldanamycin induces hsp70 and prevents α-synuclein aggregation and toxicity in vitro. *Biochem. Biophys. Res. Commun.* **321,** 665–669
36. Murphy, M. E. (2013) The HSP70 family and cancer. *Carcinogenesis* **34,** 1181–1188
37. Nylandsted, J., Brand, K., and Jäättelä, M. (2000) Heat shock protein 70 is required for the survival of cancer cells. *Ann. N.Y. Acad. Sci.* **926,** 122–125
38. Rousaki, A., Miyata, Y., Jinwal, U. K., Dickey, C. A., Gestwicki, J. E., and Zuiderweg, E. R. (2011) Allosteric drugs: the interaction of antitumor compound MKT-077 with human Hsp70 chaperones. *J. Mol. Biol.* **411,** 614–632
39. Jinwal, U. K., Miyata, Y., Koren, J., 3rd, Jones, J. R., Trotter, J. H., Chang, L., O'Leary J., Morgan, D., Lee, D. C., Shults, C. L., Rousaki, A., Weeber, E. J., Zuiderweg, E. R., Gestwicki, J. E., and Dickey, C. A. (2009) Chemical manipulation of hsp70 ATPase activity regulates tau stability. *J. Neurosci.* **29,** 12079–12088
40. Abisambra, J. F., Jinwal, U. K., Suntharalingam, A., Arulselvam, K., Brady, S., Cockman, M., Jin, Y., Zhang, B., and Dickey, C. A. (2012) DnaJA1 antagonizes constitutive Hsp70-mediated stabilization of tau. *J. Mol. Biol.* **421,** 653–661
41. Klucken, J., Shin, Y., Masliah, E., Hyman, B. T., and McLean, P. J. (2004) Hsp70 reduces α-synuclein aggregation and toxicity. *J. Biol. Chem.* **279,** 25497–25502
42. Ahmad, A. (2010) DnaK/DnaJ/GrpE of Hsp70 system have differing effects on α-synuclein fibrillation involved in Parkinson's disease. *Int. J. Biol. Macromol.* **46,** 275–279
43. Gao, X., Carroni, M., Nussbaum-Krammer, C., Mogk, A., Nillegoda, N. B., Szlachcic, A., Guilbride, D. L., Saibil, H. R., Mayer, M. P., and Bukau, B. (2015) Human Hsp70 disaggregase reverses Parkinson's-linked α-synuclein amyloid fibrils. *Mol. Cell* **59,** 781–793
44. Evans, C. G., Chang, L., and Gestwicki, J. E. (2010) Heat shock protein 70 (hsp70) as an emerging drug target. *J. Med. Chem.* **53,** 4585–4602
45. Piana, S., Lindorff-Larsen, K., and Shaw, D. E. (2011) How robust are protein folding simulations with respect to force field parameterization?. *Biophys. J.* **100,** L47–L49
46. Onufriev, A., Bashford, D., and Case, D. A. (2004) Exploring protein native states and large-scale conformational changes with a modified generalized Born model. *Proteins* **55,** 383–394
47. Eastman, P., and Pande, V. (2015) OpenMM: a hardware-independent framework for molecular simulations. *Comput. Sci. Eng.* **12,** 34–39
48. Eastman, P., Friedrichs, M. S., Chodera, J. D., Radmer, R. J., Bruns, C. M., Ku, J. P., Beauchamp, K. A., Lane, T. J., Wang, L. P., Shukla, D., Tye, T., Houston, M., Stich, T., Klein, C., Shirts, M. R., and Pande, V. S. (2013) OpenMM 4: a reusable, extensible, hardware independent library for high performance molecular simulation. *J. Chem. Theory Comput.* **9,** 461–469
49. Li, H., Robertson, A. D., and Jensen, J. H. (2005) Very fast empirical prediction and rationalization of protein pK_a values. *Proteins* **61,** 704–721
50. Bas, D. C., Rogers, D. M., and Jensen, J. H. (2008) Very fast prediction and rationalization of pK_a values for protein–ligand complexes. *Proteins* **73,** 765–783
51. Olsson, M. H., Søndergaard, C. R., Rostkowski, M., and Jensen, J. H. (2011) PROPKA3: consistent treatment of internal and surface residues in empirical pK_a predictions. *J. Chem. Theory Comput.* **7,** 525–537
52. McGibbon, R. T., Beauchamp, K. A., Harrigan, M. P., Klein, C., Swails, J. M., Hernández, C. X., Schwantes, C. R., Wang, L.-P., Lane, T. J., and Pande, V. S. (2015) MDTraj: a modern open library for the analysis of molecular dynamics trajectories. *Biophys. J.* **109,** 1528–1532
53. Swain, J. F., Schulz, E. G., and Gierasch, L. M. (2006) Direct comparison of a stable isolated Hsp70 substrate-binding domain in the empty and substrate-bound states. *J. Biol. Chem.* **281,** 1605–1611
54. Wishart, D. S., Bigam, C. G., Holm, A., Hodges, R. S., and Sykes, B. D. (1995) ^{1}H, ^{13}C and ^{15}N random coil NMR chemical shifts of the common amino acids. I. Investigations of nearest-neighbor effects. *J. Biomol. NMR* **5,** 67–81